Reprinted from

JOURNAL OF CRYSTAL GROWTH

Journal of Crystal Growth 180 (1997) 85–93

Characterization of large $KTiOPO_4$ flux grown crystals by synchrotron radiation topography

P. Rejmánková[a,*], J. Baruchel[a], P. Villeval[b], C. Saunal[b]

[a] *European Synchrotron Radiation Facility, BP 220, F-38043 Grenoble, France*
[b] *Cristal Laser, BP 44, F-54230 Chaligny, France*

Received 15 December 1996; accepted 26 February 1997

ELSEVIER

Journal of Crystal Growth

Scope of the Journal
Experimental and theoretical contributions are invited in the following fields: Theory of nucleation and growth, molecular kinetics and transport phenomena, crystallization in viscous media such as polymers and glasses. Crystal growth of metals, minerals, semiconductors, magnetics, inorganic, organic and biological substances in bulk or as thin films. Apparatus instrumentation and techniques for crystal growth, and purification methods. Characterization of single crystals by physical and chemical methods.

Abstracted/Indexed in:
Aluminium Industry Abstracts; Chemical Abstracts; Current Contents; Physical, Chemical and Earth Sciences; EI Compendex Plus; Engineered Materials Abstracts; Engineering Index; INSPEC; Metals Abstracts.

Subscription Information 1997
Volumes 170–181 of Journal of Crystal Growth (ISSN 0022-0248) are scheduled fo publication. (Frequency: semimonthly.) Prices are available from the publishers upo request. Subscriptions are accepted on a prepaid basis only. Issues are sent by SA (Surface Air Lifted) mail wherever this service is available. Airmail rates are availabl upon request. Please address all enquiries regarding orders and subscriptions to:

Elsevier Science, B.V., Order Fulfilment Department
P.O. Box 211, 1000 AE Amsterdam, The Netherlands
Tel: +31 20 485 3642; Fax: +31 20 485 3598

Claims for issues not received should be made within six months of our publicatio (mailing) date.

US mailing notice–*Journal of Crystal Growth* (ISSN 0022-0248) is published semimonthly by Elsevier Science B.V., Molenwerf 1, P.O. Box 211, 1000 AE Amsterdam, Th Netherlands. Annual subscription price in the USA is US $7081 (valid in North, Central and South America only), including air speed delivery. Periodicals postage paid at Jamaic NY 11431.
US postmasters: Send address changes to Journal of Crystal Growth, Publications Expediting, Inc., 200 Meacham Avenue, Elmont NY 11003. Airfreight and mailing in the USA b Publications Expediting.

The paper used in this publication meets the requirements of ANSI/NISO Z39.48-1992 (Permanence of Paper)

PRINTED IN THE NETHERLAND

North-Holland, an imprint of Elsevier Science

ELSEVIER

Journal of Crystal Growth 180 (1997) 85–93

JOURNAL OF CRYSTAL GROWTH

Characterization of large $KTiOPO_4$ flux grown crystals by synchrotron radiation topography

P. Rejmánková[a,*], J. Baruchel[a], P. Villeval[b], C. Saunal[b]

[a] *European Synchrotron Radiation Facility, BP 220, F-38043 Grenoble, France*
[b] *Cristal Laser, BP 44, F-54230 Chaligny, France*

Received 15 December 1996; accepted 26 February 1997

Abstract

Defects in high quality $KTiOPO_4$ single crystals grown by the flux method have been investigated by X-ray topographic techniques using synchrotron radiation. In addition to the usual observation of growth bands, growth sectors and dislocations, inversion twin boundaries and a decrease in the cell parameter c as a function of the distance from the crystal seed are reported.

PACS: 61.10.−i; 61.72.Ff; 61.72.Nn; 81.10.Dd

Keywords: Potassium titanyl phosphate; Growth by flux method; Inversion twin boundary; Synchrotron radiation topography

1. Introduction

The first crystal of potassium titanyl phosphate, $KTiOPO_4$ (KTP), was synthesized in 1890 using molten potassium pyro- and ortho-phosphate fluxes [1]. At present KTP is becoming one of the most important nonlinear optical materials for frequency doubling and waveguide devices [2]. The use of KTP in applications requires crystals of high perfection and sufficient size. Two main methods are used to produce KTP crystals: the high temperature flux method [3, 4] and the hydrothermal method [5, 6]. Conventional melt growth techniques are inappropriate since KTP decomposes partially upon melting ($T \sim 1170$°C) [7]. The flux growth process is currently the most promising to provide large KTP single crystals of high optical quality [8].

The crystal structure of KTP at room temperature belongs to the orthorhombic space group $Pna2_1$ with lattice parameters $a = 12.814$ Å, $b = 6.404$ Å and $c = 10.616$ Å [9] where the polar axis and hence the direction of spontaneous polarization is along the c-axis. KTP is a high-temperature ferroelectric with a large diversity of Curie temperatures reported (940°C ± 50°C): the phase

* Corresponding author. Fax: + 33 4 76 88 27 07; e-mail: rejma@esrf.fr.

PII S0022-0248(97)00197-8

transition temperature depends on the flux composition and crystal thermal history [10]. 180° ferroelectric domains, with domain walls lying parallel to the (1 0 0) planes, have been observed using pyroelectric, piezoelectric and electro-optical techniques on hydrothermally grown material [11]. Complex twin boundaries were found in flux-grown KTP. They are not related to the ferroelectric domains, but seem to be similar to the Dauphine twin in quartz [4]. Ferroelectric domain walls parallel to the polar axis were observed in flux [12] and hydrothermally [13] grown KTP crystals by X-ray topography, which allows determination of the three dimensional shapes of the domains.

X-ray topographic techniques were used to investigate periodically domain-inverted regions [14], electric field induced grey tracks [15] and the structural quality of flux-grown KTP crystals revealing high levels of perfection with very low dislocation densities [16, 17]. The X-ray topographs recorded on $h\,k\,l$ reflections ($l \neq 0$) under an applied electric field exhibit many dark straight lines parallel to the c-axis, the effect being maximal for $0\,0\,l$ reflections [18–20]. After removal of the field these lines gradually disappear. For an electric field perpendicular to the polar axis no effect is observed. These facts were tentatively explained by assuming that the lattice of a KTP crystal in an external electric field is distorted by the space charges associated with the formation of "polarized channels" [20].

The above examples indicate the miscellaneous applications of X-ray topography in understanding the behaviour of KTP crystals. The needs of the optoelectronics industry led to a major effort devoted to the growth process of KTP. The high quality of the produced crystals requires a characterization technique with improved sensitivity and spatial resolution to observe the weak strains which were before hidden by the general imperfection of the crystal lattice. The new possibilities offered by third generation synchrotron radiation sources like the ESRF [21] allow, in an easy way, the X-ray topographic characterization of the KTP flux-grown crystals produced by the "Cristal Laser" company. These crystals are not only of high optical quality, but they also display a high perfection even from the topographic point of view.

2. Crystal growth

The KTP crystals characterized in this study were grown by the Top-Seeded Solution Growth (TSSG) method either from $K_6P_4O_{13}$ [3, 7] or [KPO_3 + KF] [22] fluxes. The house-built "Cristal Laser" furnaces consist of three individual heating elements, a weighing device (sensitivity 1 mg) and a translation–rotation unit. The temperature is controlled within to be 0.1°C, and the gradient between the bottom of the platinum crucible and 15 cm above the melt surface is adjustable in a range of 0.1–1°C/cm. The growth units are power-secure and supervised by a computer.

The raw material $KTiOPO_4$ is dissolved in the flux and the assembly is heated to 1000°C. After stirring for homogenization, the exact saturation temperature (approximately 940°C) of the solution is determined with a test crystal during slow cooling. The seed, a KTP crystal with the dimension of 20–30 mm along the b-axis and a 3×3 to 4×4 mm^2 cross section, is immersed in the bath and rotated in the crucible off its center. The rotation axis is parallel to the b-axis and the rotation rates are in a range of 40–100 rpm. The sense of rotation is reversed every 60 s to avoid the formation of liquid inclusions [23]. The geometry of the crystal growth is schematically shown in Fig. 1a.

The supersaturation is achieved by slow cooling (1–7°C/day). The theoretical width of the metastable zone (where no homogeneous nucleation occurs) for the $K_6P_4O_{13}$ flux is approximately 6°C [24] and we have found the same result in the case of the [KPO_3 + KF] flux. In order to avoid the crystallization in the bulk of the melt and to crystallize only on the seed, one has to work within this "theoretical" metastable zone. However, the "real" metastable zone width depends on many factors, such as crucible ageing, stirring, melt purity, mechanical or thermal shocks. An heterogeneous nucleation on the inner side wall and on the bottom of the crucible during slow cooling is then prevented by using a smaller working zone width than predicted theoretically. Heterogeneous nucleation decreases the crystallization efficiency (i.e. the ratio of the mass of the main crystal over the total mass crystallized within the growth temperature range) and a small single crystal in a wide growth temperature

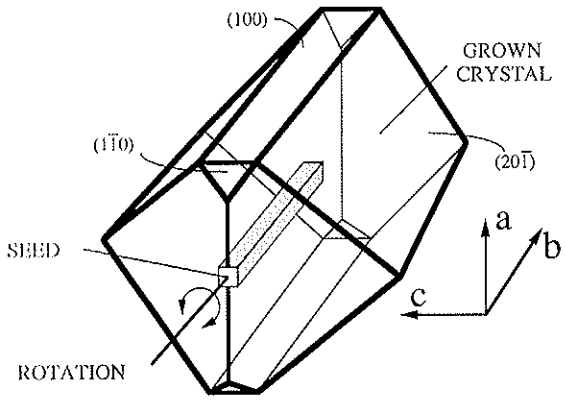

(a)

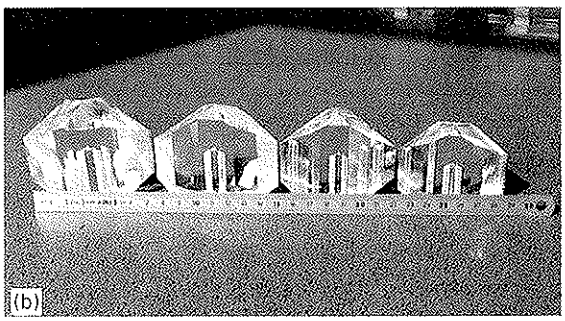

Fig. 1. (a) Schematic drawing illustrating the morphology of the KTP crystal, the location of the seed and the rotation around the *b*-axis which is systematically reversed during the crystal growth. (b) Photograph of typical KTP crystals produced by the "Cristal Laser" company, from left to right crystals of Nos. 5, 4, 3 and 2 characterized in Table 1. The seeds, elongated along the *b* axis, are clearly visible inside the crystals.

range is obtained, as shown in Table 1, crystal No. 1.

The improved control of the supersaturation and hydrodynamic processes through slow cooling and crystal rotation [25] allows, after four weeks, the growth of a raw crystal up to 300 g weight. Crystallization efficiencies up to 95% are achieved and at the present, crystal sizes and quality are mainly limited by the crucible capacity. Table 1 summarizes the growth conditions, including this crucial crucible size, and Fig. 1b shows the photograph of typical produced KTP crystals.

3. Experimental procedure

The crystalline quality of the KTP crystals was investigated at the BM5 "Optics" and at the ID19 "Topography" beamlines at the European Synchrotron Radiation Facility (Grenoble, France) by white beam synchrotron radiation diffraction topography in transmission mode. The projection and section topographs were recorded as Laue patterns (each spot corresponds to a topograph) on Kodak Industrex SR films with typical exposure times of 1 and 20 s, respectively [21]. Note that in the case of the projection topographs a chopper decreasing the incident beam intensity by the factor 20 was used in order to reduce the heat load on the sample [26]. When recording the section topographs (the experimental set up is schematically shown on Fig. 2) this device is usually not needed due to the small illuminated volume. The crystal-to-film distance was

Table 1
Typical growth conditions and characteristics of produced KTP crystals

Crystal No.	Crucible size diameter × height (mm^2)	Growth duration (days)	Growth temperature range (°C)	Crystal weight (g)	Crystal size (mm^3)	Crystallization efficiency (%)
1	120 × 80	40	266	81	25 × 37 × 54	20
2	120 × 120	25	91	151	25 × 53 × 63	60
3	120 × 80	27	110	182	27 × 56 × 70	80
4	120 × 80	25	105	216	25 × 60 × 76	80
5	150 × 100	28	71	300	35 × 67 × 76	80
6	120 × 100	35	52	140	25 × 40 × 62	95

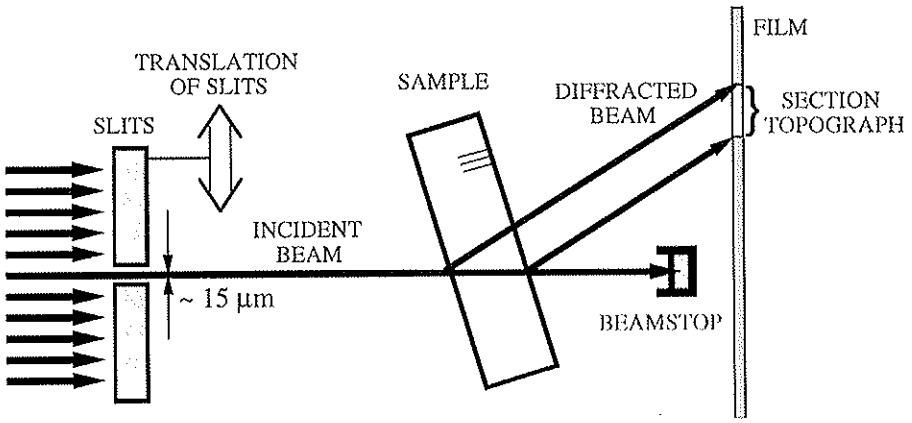

Fig. 2. Experimental arrangement for section topographs with the possibility to modify the incident beam position on the sample by the displacement of the slits.

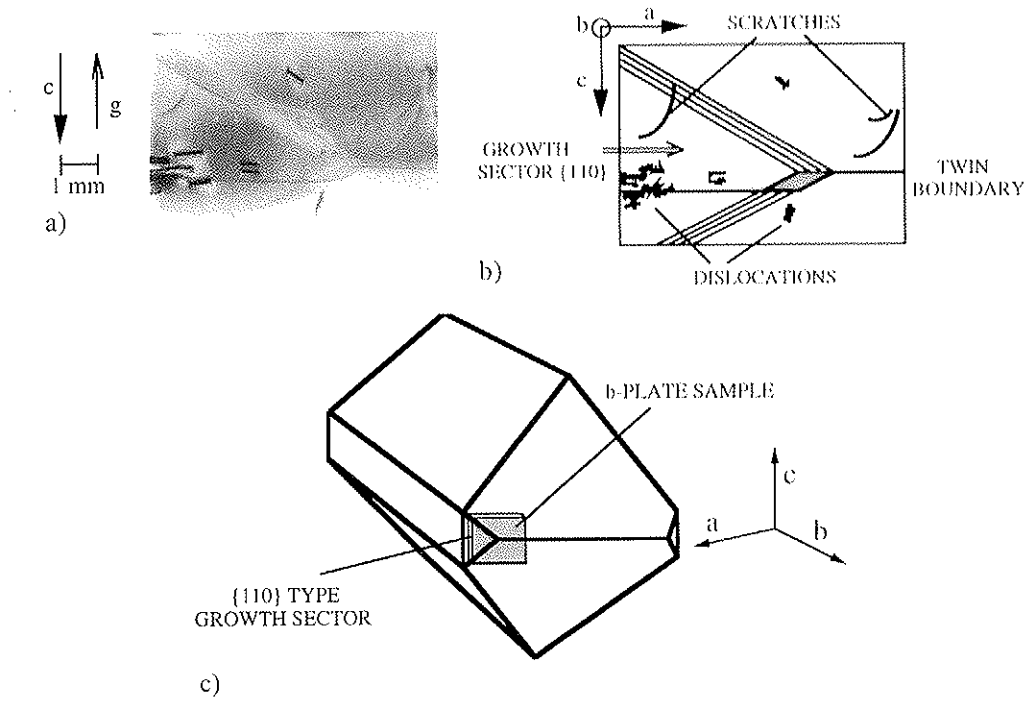

Fig. 3. (a) Projection topograph of the b-plate, reflection 1 1 3, $\mu t \sim 0.4$, $\lambda = 0.28$ Å, $t \sim 0.9$ mm, μ is the absorption coefficient and t is the thickness of the sample, g is the projection of the diffraction vector on the film. (b) Scheme of the topograph indicating the location of the features discussed in the text. (c) Location of the investigated b-plate sample in the grown crystal.

in the order of 20 cm. The combination of information obtained from section and projection topographs recorded on one sample allows the determination of the three-dimensional shape of a given defect inside the crystal [27].

The investigated samples were a-, b- and c-plates, i.e. they have been cut respectively, perpendicularly to the a, b and c crystal axis. The a-plates show similar behaviour as the b-plates. We present the results obtained on three samples exhibiting typical, and interesting, features: one b-plate and two c-plates. The b-plate was cut quite far (more than 1 cm) from the seed and is 0.9 mm thick. The c-plates, 1 and 1.8 mm thick, were cut through the seed and cross the whole grown crystal.

4. X-ray topographic studies

Fig. 3a shows a 1 1 3 projection topograph of the b-plate crystal. The schematic diagram of the topograph in Fig. 3b, shows a growth sector lying along {1 1 0} type planes (displaying a triangular form), dislocations, surface scratches and a straight line parallel to the a-axis with a small "jump" in the c direction where crossing the boundary of {1 1 0} growth sector. Fig. 3c indicates the location of the investigated sample with respect to the {1 1 0} type growth sector observed on the topograph. The dislocation density of the slice is very low, being around 10 cm^{-2} in the central part of the {1 1 0} sector and outside this sector the sample is nearly dislocation-free. We have followed the location of the planar defect (corresponding to the straight line on the traverse topographs) inside the sample using the section topographs recorded with the slits set perpendicularly to the a-axis with different positions of the incident beam on the crystal [27]. The interface orientations were determined to be {0 1 3} outside the growth sector {1 1 0}, {0 2 3} at the "jump" and {0 1 4} inside the {1 1 0} sector.

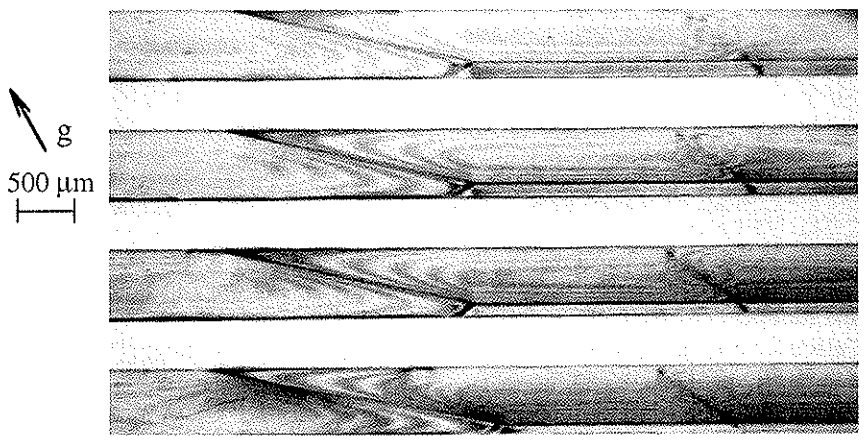

a)

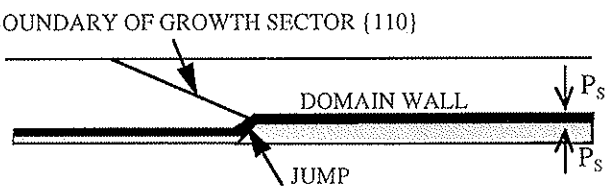

b)

Fig. 4. (a) Section topographs of the c-plate, reflection $\bar{1}\,5\,\bar{2}$, $\mu t \sim 0.7$, $\lambda = 0.32$ Å, $t \sim 1.8$ mm, slits set perpendicularly to the b-axis, the a-axis is horizontal on the figure. (b) Schematic drawing of the topograph with its main features, P_S indicates the direction of the spontaneous polarization.

This straight line is invisible for 0 0 l reflections, but is clearly visible even for these reflections, when a weak DC field (~20 V/cm) is applied along the c-axis, as the contrast of the striations produced by the field reverses when crossing it [20].

We propose that this planar defect corresponds to an inversion twin boundary. The twins are related by a 180° rotation around [0 1 0] direction, or, more briefly expressed, by the operation 2[0 1 0], as indicated in Ref. [28]. The inversion twin boundary separates regions where the spontaneous polarization is reversed and could result from the reversal of the rotation of the seed in the liquid bath during the crystal growth process [29]. The whole crystal is divided at the level of the seed into two large domains by a charged ferroelectric domain wall, which is perpendicular to the polar axis.

The same ferroelectric domains related feature, is shown on the section topographs of Fig. 4a, this time on the 1.8 mm thick c-plate cut through the seed. The slits were set perpendicularly to the b-axis for different positions of the incident beam on the crystal. The schematic drawing of the topograph, given in Fig. 4b, indicates the boundary of growth sector {1 1 0} producing again a "jump" on the interface of domains. Note the presence of Kato's or Pendellösung fringes [30] on the topographs. They indicate a very high crystalline quality, and display an independent pattern in each part of the sample separated by the growth sector boundary as in the case of two independent edge-shaped crystals. When a DC electric field was applied along the c-axis, a strong enhancement of intensity has been observed in the neighbourhood of the domain wall indicating the presence of a strain field produced by ionic flow across this interface. No displacement of the domain wall was observed, a feature which could be related to the trapping effect of the {1 1 0} growth defects. The {1 1 0} faces of grown crystal can disappear if the relative growth speed is slightly modified and consequently the crystal is grown outside the metastable zone [25]. The presence of {1 0 0} type growth sectors indicates in this way a high quality of the grown crystal.

Fig. 5 presents a typical c-plate cut through the seed. The schematic diagram of Fig. 5a indicates the main features observed and the locations of the

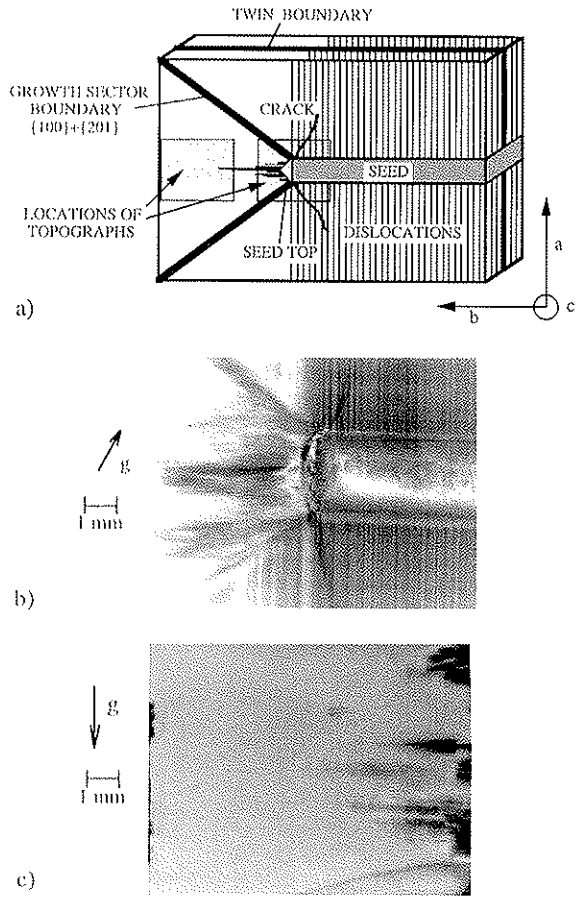

Fig. 5. (a) Scheme of the c-plate cut through the seed, dimensions $25 \times 40 \times 1$ mm^3. (b) Projection topograph of the region around the end of the seed, reflection $5\,\bar{2}\,1$, $\mu t \sim 0.7$, $\lambda = 0.38$ Å. (c) Projection topograph of the region far (>1 cm) from the seed, reflection $\bar{2}\,0\,0$, $\mu t \sim 1.3$, $\lambda = 0.49$ Å with the contribution of the reflection $\bar{4}\,0\,0$, $\mu t \sim 0.3$, $\lambda = 0.25$ Å.

recorded topographs, shown in Fig. 5b and Fig. 5c. The end of the seed and its neighbourhood is shown on Fig. 5b. On the right part of the topograph many dislocations parallel to the a-axis are visible, starting from the surface of the seed and crossing the whole crystal. The images of the dislocations parallel to the b-axis disappear gradually when going away from the seed. The origin of these dislocations is the top of the seed, which is a highly distorted region, partly filled by the flux. At a distance of about 1 cm from the top of the seed the

crystal is nearly defect-free, as shown in Fig. 5c, and Kato's fringes were observed on the corresponding section topographs. The {1 0 1} plane boundaries between the {1 0 0} and {2 0 1} growth sectors were observed as two straight diagonal bands starting from the corners of the seed. The volume of a grown crystal defined by these {1 0 1} boundaries is the region of best crystalline quality if far enough from the seed.

The dislocations parallel to the *a*-axis start clearly from the surface of the seed, and are only present at the level of the seed, the rest of the crystal being nearly dislocations-free. When the seed itself contains dislocations, they generally do not continue in the grown crystal. These dislocations are not observed on topographs performed using the (*h* 0 0) reflecting planes. Their Burgers' vector is consequently perpendicular to the *a*-axis, and they are pure edge dislocations. These [1 0 0] edge dislocations could originate on irregularities of the seed surface etched before the crystal growth. The section topographs of the 1 mm thick c-plate shown in Fig. 6 suggest the influence of the surface-seed inhomogeneities on the distribution of dislocations within the grown crystal. The first section corresponds to the "quasi-perfect" central part of the seed. The second section was recorded just at the level of the seed surface and shows a quantity of diagonal lines corresponding probably to the strains remaining near to the seed surface after etching. The third and the forth sections were recorded on the grown crystal and repeat, through the dislocation images (dots), the same defects seen on the second section.

Fig. 7a shows section topographs recorded at different positions of the incident beam on the seed of the c-plate 1.8 mm thick sample, with slits set perpendicularly to the *a*-axis. The section topographs corresponding to the reflections above the direct beam spot show the upper and lower part of the seed to be contracted and expanded, respectively. This behaviour can be explained by a curvature of the reflecting planes of the seed, schematically represented in Fig. 7b, produced by a smaller lattice parameter c of the grown crystal. These sections thus indicate that the seed has a bigger lattice parameter c than the grown crystal, $\Delta c/c$ being estimated to be 10^{-4}–10^{-3}. This value was

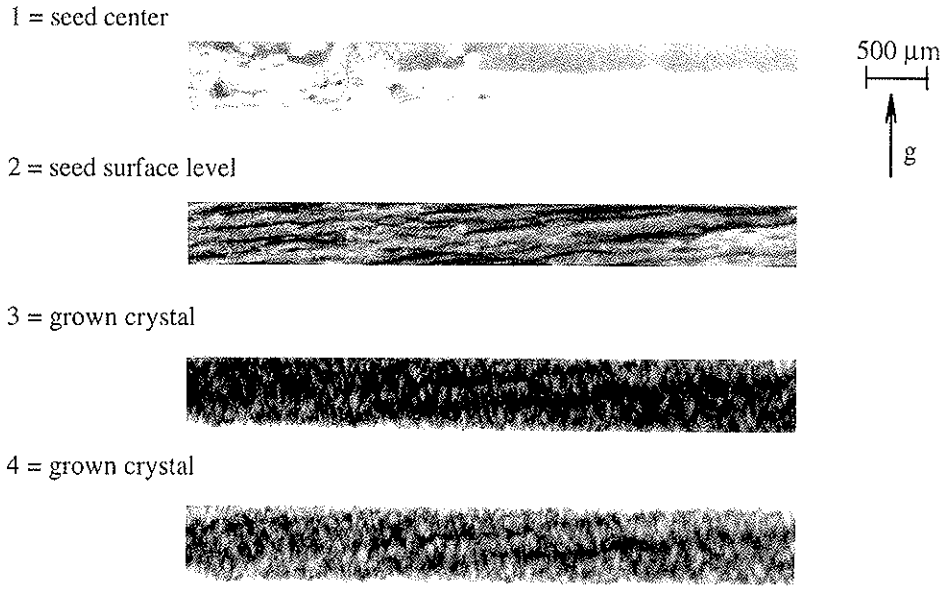

Fig. 6. Section topographs of the c-plate corresponding to the two different locations on the seed (1 = central, 2 = surface part) and two locations (3, 4) on the grown crystal in order to follow the surface seed irregularities within the grown crystal. Slits set perpendicularly to the *a*-axis, the *b*-axis is horizontal on the figure, the separation of the sections is 1 mm, reflection 6 0 1, $\mu t \sim 2.7$, $\lambda = 0.54$ Å, $t \sim 1.8$ mm.

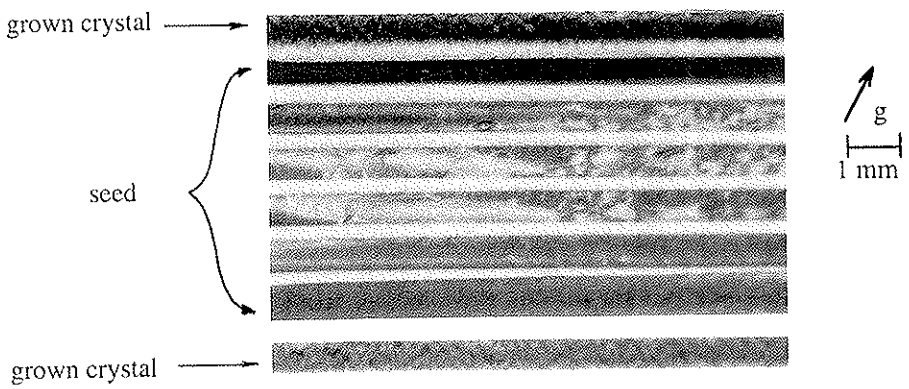

a)

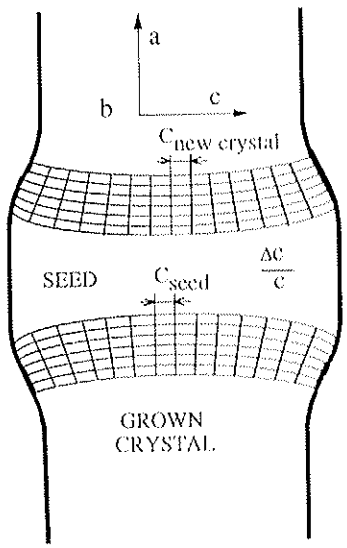

b)

Fig. 7. (a) Section topographs at different places of the seed of the c-plate, 1 mm thick, slits set perpendicularly to the a-axis, the b-axis is horizontal on the figure, the separation of the sections is 0.5 mm, reflection 713, $\mu t \sim 0.3$, $\lambda = 0.27$ Å. (b) Schematic drawing of curved planes of the seed produced by smaller lattice parameter c of the grown crystal.

obtained from the expansion/contraction of the grown crystal section topograph with respect to the seed ones, and the known crystal-to-film distance (23.5 cm). The misorientation angle α was thus calculated and it is worth, in the case of the 713 reflection (Fig. 7a), approximately 1.8×10^{-4} rad. The corresponding lattice mismatch $\Delta c/c$ is equal to $\alpha/\cos\phi \sin\phi$, with ϕ the angle between the crystal surface and the diffracting planes.

5. Conclusions

The crystalline perfection of KTP crystals prepared using the described top seeded, slow cooling technique, is very high on large areas. Indeed, on the section topographs of the areas of crystal located far enough from the seed, the characteristic Kato's fringes appear, indicating a very high crystalline quality of these parts of crystal.

Nevertheless, the defects as growth sector boundaries and dislocations reduce the useful volume for applications in nonlinear optics. The dislocations along [1 0 0] seem to be related to the irregularities of the surface of the seed. The lattice mismatch between the seed and the grown crystal for the parameter c can be estimated to be 10^{-4}–10^{-3} with the c spacing of the grown crystal being smaller. Further investigations by high resolution diffraction are foreseen to measure more precisely this lattice mismatch. We have characterized the boundary between the twins correlated by the operation 2[0 1 0], corresponding to a charged ferroelectric domain wall. The inversion twin boundary is generated during the crystal growth process and the whole crystal is divided into two large ferroelectric domains. The domains are, however, so large that optical devices can be cut from a single domain part of crystal.

Acknowledgements

The crystal-growth part of this work was supported by the 'Direction de la Recherche Et de la Technologie (DRET)', contract No. 95-346.

References

[1] M.L. Ouvrard, Comptes Rendus 111 (1890) 177, quoted in Ref. [2].
[2] J.C. Jacco, J. Proc. Photo-Opt. Instrum. Eng. 968 (1988) 93.
[3] P.F. Bordui, J.C. Jacco, G.M. Loiacono, R.A. Stolzenberger, J.J. Zola, J. Crystal Growth 84 (1987) 403.
[4] G.M. Loiacono, R.A. Stolzenberger, Appl. Phys. Lett. 53 (1988) 1498.
[5] E.C. Zumsteg, J.D. Bierlein, T.E. Gier, J. Appl. Phys. 47 (1976) 4980.
[6] F. Ahmed, R.F. Belt, G. Gashurov, J. Appl. Phys. 60 (2) (1986) 839.
[7] J.C. Jacco, G.M. Lioacono, M. Jaso, G. Mizell, B. Greenberg, J. Crystal Growth 70 (1984) 484.
[8] T. Sasaki, A. Miyamoto, A. Yokotani, S. Nakai, J. Crystal Growth 128 (1993) 950.
[9] I. Tordjman, R. Masse, J.C. Guitel, Z. Krist. 139 (1974) 103.
[10] N. Angert, M. Tseitlin, E. Yashchin, M. Roth, Appl. Phys. Lett. 67 (13) (1995) 1941.
[11] J.D. Bierlein, F. Ahmed, Appl. Phys. Lett. 51 (17) (1987) 1322.
[12] S. Wang, M. Dudley, L.K. Cheng, J.D. Bierlein, Mater. Res. Soc. Symp. Proc. 307 (1993) 243.
[13] S. Wang, M. Dudley, L.K. Cheng, J.D. Bierlein, W. Bindloss, Mater. Res. Soc. Symp. Proc. 310 (1993) 29.
[14] Z.W. Hu, P.A. Thomas, M.C. Gupta, W.P. Risk, Appl. Phys. Lett. 66 (1) (1995) 13.
[15] M.N. Satyanarayan, H.L. Bhat, M.R. Srinivasan, P. Ayyub, M.S. Multani, Appl. Phys. Lett. 67 (19) (1995) 2810.
[16] R.J. Bolt, H. de Haas, M.T. Sebastian, H. Klapper, J. Crystal Growth 110 (1991) 587.
[17] P.J. Halfpenny, L. O'Neill, J.N. Sherwood, G.S. Simpson, A. Yokotani, A. Miyamoto, T. Sasaki, S. Nakai, J. Crystal Growth 113 (1991) 722.
[18] M.T. Sebastian, H. Klapper, R.J. Bolt, J. Appl. Crystal. 25 (1992) 274.
[19] L.G. Tian, X.G. Han, R.S. Li, J.Y. Chen, Acta Crystallogr. A 49, Supplement C-515 XVI, Int. Conf. Crystallography, Beijing, China, 1993, p. 360.
[20] P. Rejmánková, J. Baruchel, J. Kulda, Phil. Mag. B, 1997, in press.
[21] R. Barrett, J. Baruchel, J. Härtwig, F. Zontone, J. Phys. D 28 (1995) A250.
[22] G. Marnier, Brevet France No. 8511520, 26 July 1985; US Patent No. 4746396, 24 May 1988.
[23] P.F. Bordui, S. Motakef, J. Crystal Growth 96 (1989) 405.
[24] F.J. Kumar, D. Jayaraman, C.C. Subramanian, P. Ramasamy, J. Crystal Growth 137 (1994) 535.
[25] C. Saunal, PhD Thesis, Dept. of Materials Science, University of Nancy, 1995.
[26] F. Zontone, L. Mancini, Nuovo Cimento (1997), in press.
[27] C. Medrano, P. Rejmánková, M. Ohler, I. Matsouli, Nuovo Cimento (1997), in press.
[28] P.A. Thomas, A.M. Glazer, J. Appl. Crystallogr. 24 (1991) 968.
[29] D. Lupinski, P. Villeval, unpublished.
[30] N. Kato, A. Lang, Acta Crystallogr. 12 (1959) 787.